JOURNAL OF MATERIALS SCIENCE 41 (2006) 217–228

Loss mechanisms and high power piezoelectrics

K. UCHINO, J. H. ZHENG, Y. H. CHEN, X. H. DU, J. RYU, Y. GAO, S. URAL, S. PRIYA
International Center for Actuators and Transducers, Penn State University, University Park, PA, USA

S. HIROSE
Faculty of Eng., Yamagata University, Yonezawa, Japan

Heat generation is one of the significant problems in piezoelectrics for high power density applications. In this paper, we review the loss mechanisms in piezoelectrics first, followed by the heat generation processes for various drive conditions. Heat generation at off-resonance is caused mainly by dielectric loss tan δ' (i.e., P-E hysteresis loss), not by mechanical loss, while the heat generation at resonance is mainly attributed to mechanical loss tan ϕ'. Then, practical high power materials developed at Penn State is introduced, which exhibit the vibration velocity more than 1 m/s, leading to the power density capability 10 times of the commercially available "hard" PZTs. We propose a internal bias field model to explain the low loss and high power origin of these materials. Finally, using a low temperature sinterable "hard" PZT, we demonstrated a high power multilayer piezoelectric transformers.

1. Intoduction

Loss or hysteresis in piezoelectrics exhibits both merits and demerits. For positioning actuator applications, hysteresis in the field-induced strain provides a serious problem, and for resonance actuation such as ultrasonic motors, loss generates significant heat in the piezoelectric materials. Further, in consideration of the resonant strain amplified in proportion to a mechanical quality factor, low (intensive) mechanical loss materials are preferred for ultrasonic motors. To the contrary, for force sensors and acoustic transducers, a low mechanical quality factor Q_m (which corresponds to high mechanical loss) is essential to widen a frequency range for receiving signals.

K. H. Haerdtl wrote a review article on electrical and mechanical losses in ferroelectric ceramics [1]. Losses are considered to consist of four portions: (1) domain wall motion, (2) fundamental lattice portion, which should also occur in domain-free monocrystals, (3) microstructure portion, which occurs typically in polycrystalline samples, and (4) conductivity portion in highly-ohmic samples. However, in the typical piezoelectric ceramic case, the loss due to the domain wall motion exceeds the other three contributions significantly. They reported interesting experimental results on the relationship between electrical and mechanical losses in piezoceramics, $Pb_{0.9}La_{0.1}(Zr_{0.5}Ti_{0.5})_{1-x}Me_xO_3$, where Me represents the doped ions Mn, Fe or Al and x varied between 0 and 0.09. However, they measured the mechanical losses on poled ceramic samples, while the electrical losses on unpoled samples, i.e., in a different polarization state, which lead big ambiguity in the discussion.

Authors are aware little systematic studies of the loss mechanisms in piezoelectrics, particularly in high electric field and high power density ranges. Although T. Ikeda described part of the formulas of this paper in his textbook [2], he totally neglected the piezoelectric losses, which have been found not to be neglected in our investigations. In this paper, we review the loss mechanisms in piezoelectrics first, followed by the heat generation processes for various drive conditions. Then, practical high power materials developed at Penn State are introduced, exhibiting the power density capability 10 times of the commercially available "hard" PZTs. We propose a model to explain the low loss and high power origin of these materials.

0022-2461
DOI: 10.1007/s10853-005-7201-0

Finally, using a low temperature sinterable "hard" PZT, we demonstrated a high power multilayer piezoelectric transformers.

The terminologies, "intensive" and "extensive" losses are introduced in the relation with "intensive" and "extensive" parameters in the phenomenology. These are not directly relevant with "intrinsic" and "extrinsic" losses which were introduced to explain the loss contribution from the mono-domain single crystal status and from the others [3]. In this paper, our discussion is focused on the "extrinsic" losses, in particular, domain-reorientation originated losses.

2. General consideration of loss and hysteresis in piezoelectrics

2.1. Theoretical formulas

Since we have described the detailed mathematics in the previous paper [4], we just summarize the results in this section. We start from the following two piezoelectric equations:

$$x = s^{\mathrm{E}} X + d\,E, \tag{1}$$

$$D = d\,X + \varepsilon^{\mathrm{X}} \varepsilon_0 E. \tag{2}$$

Here, x is strain, X, stress, D, electric displacement, E, electric field. Equations 1 and 2 are the expression in terms of intensive (i.e., externally controllable) physical parameters X and E. The elastic compliance s^{E}, the dielectric constant ε^{X} and the piezoelectric constant d are temperature-dependent. Note that the piezoelectric equations cannot yield a delay-time related loss, without taking into account irreversible thermodynamic equations or dissipation functions, in general. However, the latter considerations are mathematically equivalent to the introduction of complex physical constants into the phenomenological equations, if the loss is small and can be treated as a perturbation.

Therefore, we will introduce complex parameters $\varepsilon^{\mathrm{X}^*}$, s^{E^*} and d^* in order to consider the hysteresis losses in dielectric, elastic and piezoelectric coupling energy:

$$\varepsilon^{\mathrm{X}^*} = \varepsilon^{\mathrm{X}}(1 - j\,\tan\,\delta'), \tag{3}$$

$$s^{\mathrm{E}^*} = s^{\mathrm{E}}(1 - j\,\tan\,\phi'), \tag{4}$$

$$d^* = d(1 - j\,\tan\,\theta'). \tag{5}$$

θ' is the phase delay of the strain under an applied electric field, or the phase delay of the electric displacement under an applied stress. Both delay phases should be exactly the same if we introduce the same complex piezoelectric constant d^* into Equations 1 and 2. δ' is the phase delay of the electric displacement to an applied electric field under a constant stress (e.g., zero stress) condition, and ϕ' is the phase delay of the strain to an applied stress under a constant electric field (e.g., short-circuit) condition. We will consider these phase delays as "intensive" losses.

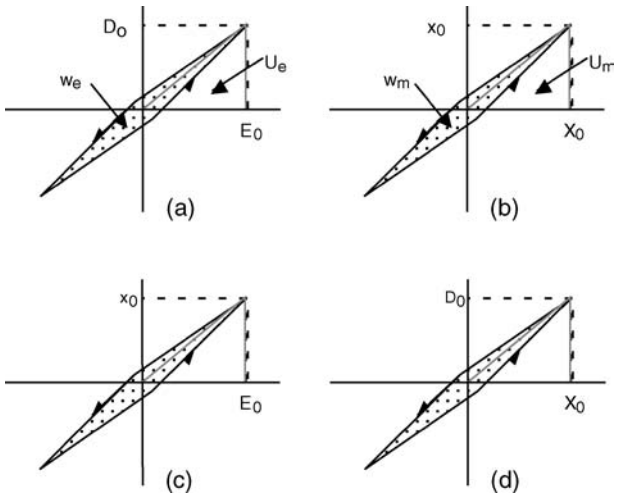

Figure 1 (a) D vs. E (stress free), (b) x vs. X (short-circuit), (c) x vs. E (stress free) and (d) D vs. X (short-circuit) curves with a slight hysteresis in each relation.

Fig. 1a–d correspond to the model hysteresis curves for practical experiments: D vs. E curve under a stress-free condition, x vs. X under a short-circuit condition, x vs. E under a stress-free condition and D vs. X under a short-circuit condition for measuring current, respectively. Notice that these measurements are easily conducted in practice.

The stored energies and hysteresis losses for pure dielectric and elastic energies can be calculated as:

$$U_{\mathrm{e}} = (1/2)\varepsilon^{\mathrm{X}}\varepsilon_0 E_0^2, \tag{6}$$

$$w_{\mathrm{e}} = \pi\varepsilon^{\mathrm{X}}\varepsilon_0 E_0^2\,\tan\,\delta', \tag{7}$$

$$U_{\mathrm{m}} = (1/2)s^{\mathrm{E}} X_0^2, \tag{8}$$

$$w_{\mathrm{m}} = \pi s^{\mathrm{E}} X_0^2\,\tan\,\phi'. \tag{9}$$

The electromechanical hysteresis losses are more complicated, which can be calculated as follows, depending on the measuring ways; when measuring the induced strain under an electric field,

$$U_{\mathrm{em}} = (1/2)(d^2/s^{\mathrm{E}})E_0^2, \tag{10}$$

and

$$w_{\mathrm{em}} = \pi(d^2/s^{\mathrm{E}})E_0^2(2\,\tan\,\theta' - \tan\,\phi'). \tag{11}$$

Note that the strain vs. electric field measurement should provide the combination of piezoelectric loss $\tan\,\theta'$ and

elastic loss tan ϕ'. When we measure the induced charge under stress, the stored energy U_{me} and the hysteresis loss W_{me} during a quarter and a full stress cycle, respectively, are obtained as

$$U_{me} = (1/2)(d^2/\varepsilon_0\varepsilon^X)X_0^2, \tag{12}$$

$$w_{me} = \pi(d^2/\varepsilon_0\varepsilon^X)X_0^2(2\tan\theta' - \tan\delta'). \tag{13}$$

Hence, from the measurements of D vs. E and x vs. X, we obtain tan δ' and tan ϕ', respectively, and either the piezoelectric (D vs. X) or converse piezoelectric measurement (x vs. E) provides tan θ' through a numerical subtraction.

So far, we discussed the "intensive" dielectric, mechanical and piezoelectric losses in terms of "intensive" parameters X and E. In order to consider real physical meanings of the losses in the material, we will introduce the "extensive" losses [4] in terms of "extensive" parameters x and D. In practice, intensive losses are easily measurable, but extensive losses are not, but obtainable from the intensive losses. When we start from the piezoelectric equations in terms of extensive physical parameters x and D:

$$X = c^D x - h\,D, \tag{14}$$

$$E = -hx + \kappa^x\kappa_0 D, \tag{15}$$

we introduce the extensive dielectric, elastic and piezoelectric losses as

$$\kappa^{x*} = \kappa^x(1 + j\tan\delta), \tag{16}$$

$$c^{D*} = c^D(1 + j\tan\phi), \tag{17}$$

$$h^* = h(1 + j\tan\theta). \tag{18}$$

It is notable that the permittivity under a constant strain (e.g., zero strain or completely clamped) condition, ε^{x*} and the elastic compliance under a constant electric displacement (e.g., open-circuit) condition, s^{D*} can be provided as an inverse value of κ^{x*} and c^{D*}, respectively, in this simplest one dimensional expression (in the case of a general 3-D expression, this part must be translated as "inverse matrix components of κ^{x*} and c^{D*} tensors."). Thus, using the exactly the same losses in Equations 16 and 17,

$$\varepsilon^{x*} = E^x(1 - j\tan\delta), \tag{19}$$

$$s^{D*} = s^D(1 - j\tan\phi), \tag{20}$$

We will consider these phase delays again as "extensive" losses.

Here, we consider the physical property difference between the boundary conditions; E constant and D constant, or X constant and x constant in a simplest 1-D model. When an electric field is applied on a piezoelectric sample as illustrated in the top of Fig. 2, this state will be equivalent to the superposition of the following two steps: first, the sample is completely clamped and the field E_0 is applied (pure electrical energy (1/2) $\varepsilon^x\varepsilon_0\ E_0^2$ is input); second, keeping the field at E_0, the mechanical constraint is released (additional mechanical energy (1/2) $(d^2/s^E)E_0^2$ is necessary). The total energy should correspond to the total input electrical energy (1/2) $\varepsilon^X\varepsilon_0\ E_0^2$. Similar energy calculation can be obtained from the bottom of Fig. 2, leading to the following equations:

$$\varepsilon^x/\varepsilon^X = (1 - k^2), \tag{21}$$

$$s^D/s^E = (1 - k^2), \tag{22}$$

$$\kappa^X/\kappa^x = (1 - k^2), \tag{23}$$

$$c^E/c^D = (1 - k^2), \tag{24}$$

where

$$k^2 = d^2/(s^E\varepsilon_0\varepsilon^X) = h^2/(c^D\kappa^x\kappa_0). \tag{25}$$

This k is called the *electromechanical coupling factor*, which is defined as a real number in this manuscript.

In order to obtain the relationships between the intensive and extensive losses, the following three equations are essential:

$$\varepsilon_0\varepsilon^X = [\kappa^x\kappa_0(1 - h^2/(c^D\kappa^x\kappa_0))]^{-1}, \tag{26}$$

$$s^E = [c^D(1 - h^2/(c^D\kappa^x\kappa_0))]^{-1}, \tag{27}$$

$$d = [h^2/(c^D\kappa^x\kappa_0)][h(1 - h^2/(c^D\kappa^x\kappa_0))]^{-1}. \tag{28}$$

Replacing the parameters in Equations 26 and 27 by the complex parameters in Equations 3, 5), 16–18, we obtain the relationships between the intensive and extensive losses:

$$\tan\delta' = (1/(1 - k^2))[\tan\delta + k^2(\tan\phi - 2\tan\theta)], \tag{29}$$

$$\tan\phi' = (1/(1 - k^2))[\tan\phi + k^2(\tan\delta - 2\tan\theta)], \tag{30}$$

$$\tan\theta' = (1/(1 - k^2))[\tan\delta + \tan\phi + (1 + k^2)\tan\theta], \tag{31}$$

where k is the electromechanical coupling factor defined by Equation 25, and here as a real number. It is important

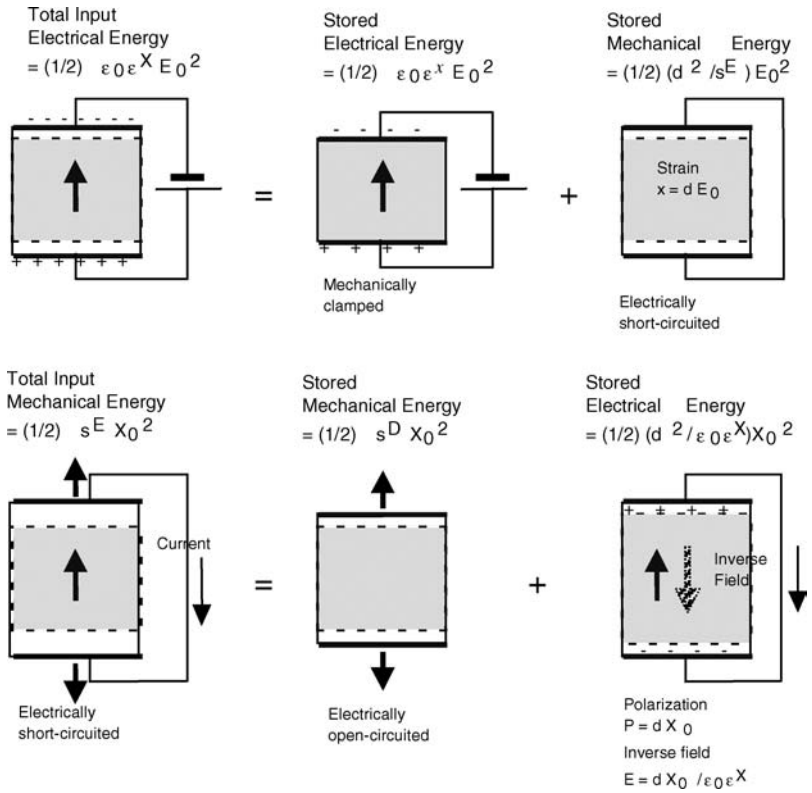

Figure 2 Conceptual figure for explaining the relation between ε^{X} and ε^{x}, s^{E} and s^{D}

that the intensive dielectric and elastic losses are mutually correlated with the extensive dielectric, elastic and piezoelectric losses through the electromechanical coupling k^2, and that the denominator $(1-k^2)$ comes basically from the ratios, $\varepsilon^x/\varepsilon^X = (1-k^2)$ and $s^D/s^E = (1-k^2)$, and this real part reflects to the dissipation factor when the imaginary part is divided by the real part.

2.2. Experimental example

We determined "intensive" dissipation factors first from (a) D vs. E (stress free), (b) x vs. X (short-circuit), (c) x vs. E (stress free) and (d) D vs. X (short-circuit) curves for a soft PZT based multilayer actuator [5]. Then, we calculated the "extensive" losses as shown in Fig. 3. Note that the piezoelectric losses $\tan\theta'$ and $\tan\theta$ are not so small as previously believed, but comparable to the dielectric and elastic losses, and increase gradually with the field or stress. Also it is noteworthy that the extensive dielectric loss $\tan\delta$ increases significantly with an increase of the intensive parameter, i.e., the applied electric field, while the extensive elastic loss $\tan\phi$ is rather insensitive to the intensive parameter, i.e., the applied compressive stress. When similar measurements to Fig.1a and b, but under constrained conditions; that is, D vs. E under a completely clamped state, and x vs. X under an open-circuit state, respectively, we can expect smaller hystereses; that is, extensive losses, $\tan\delta$ and $\tan\phi$. These measurements seem to be alternative methods to determine the three losses separately, however, they are rather difficult in practice.

2.3. Physical meaning of extensive losses

For making the situation simplest, we consider here only the domain wall motion-related losses. Taking into account the fact that the polarization change is primarily attributed to 180 degree domain wall motion, while the strain is attributed to 90 degree (or non-180°) domain wall motion, we suppose that the extensive dielectric and mechanical losses are originated from 180° and 90° domain wall motions, respectively, as illustrated in Fig. 4. The dielectric loss comes from the hysteresis during the 180° polarization reversal under E, while the elastic loss comes from the hysteresis during the 90° polarization reorientation under X. In this model, the intensive (observable) piezoelectric loss is explained by the 90° polarization reorientation under E, which can be realized by superimposing the 90° polarization reorientation under X and the 180° polarization reversal under E. This is the primarily reason why Equation 11 includes a combination term as $(2\tan\theta' - \tan\phi')$.

If we adopt the Uchida-Ikeda polarization reversal/reorientation model [6], we can explain the loss change with intensive parameter (externally controllable parameter). By finding the polarization P and the field-induced

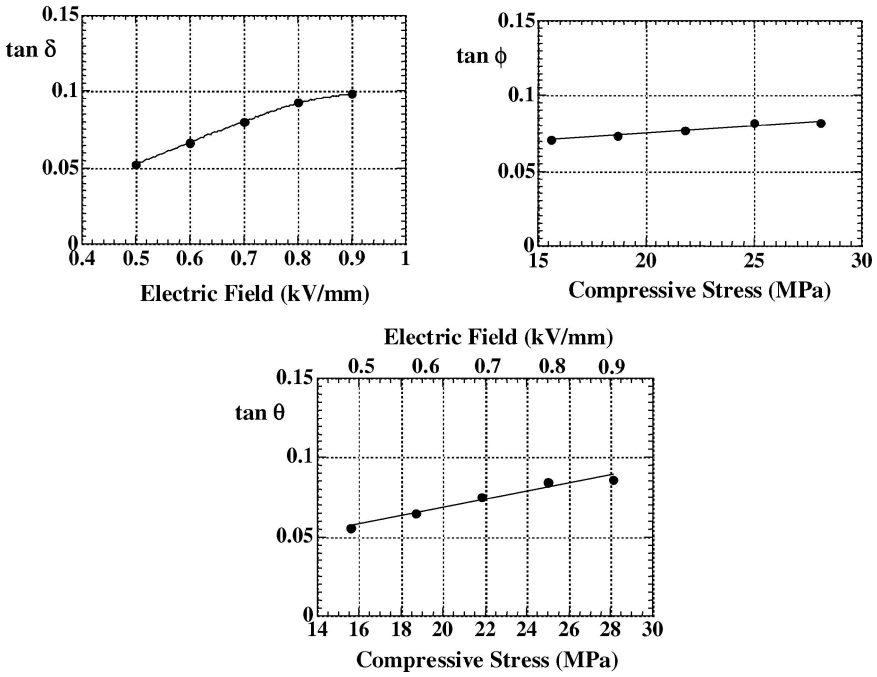

Figure 3 Extensive loss factors, tan δ, tan ϕ and tan θ as a function of electric field or compressive stress, measured for a PZT based actuator.

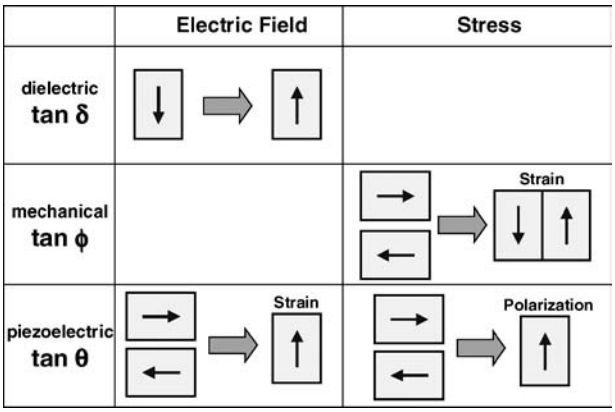

Figure 4 Polarization reversal/reorientation model for explaining dielectric, elastic and piezoelectric losses.

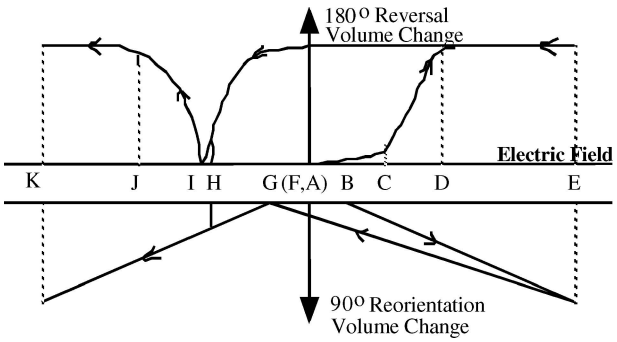

Figure 5 Polarization reversal/reorientation model for explaining the loss change with electric field.

strain x as a function of the electric field E, it is possible to estimate the volume in which a 180° reversal or a 90° rotation occurred. This is because the 180° domain reversal does not contribute to the induced strain, only the 90° rotation does, whereas the 180° domain reversal contributes mainly to the polarization. The volume change of the domains with external electric field is shown schematically in Fig. 5 that with the application of an electric field the 180° reversal occurs rapidly whereas the 90° rotation occurs slowly. It is notable that at G in the figure, there remains some polarization while the induced strain is zero, at H the polarizations from the 180° and 90° reorientations cancel each other and become zero, but the strain is not at its minimum. Due to a sudden change in 180° reversal above a certain electric field, we can expect a sudden increase in the polarization hysteresis and in the loss [this may reflect to the extensive dielectric loss measurement in Fig. 3 top left]; while the slope of 90° reorientation is almost constant, we can expect a constant loss or a mechanical quality factor Q_m with changing the external parameter, E or X [extensive elastic loss in Fig. 3 top right]. This situation will be discuss again in the later section.

3. Losses at a piezoelectric resonance

So far, we have considered the losses for a quasi-static or off-resonance state. Problems in ultrasonic motors which are driven at the resonance frequency include significant distortion of the admittance frequency spectrum due to nonlinear behavior of elastic compliance at a high vibration amplitude, and heat generation which causes a serious degradation of the motor

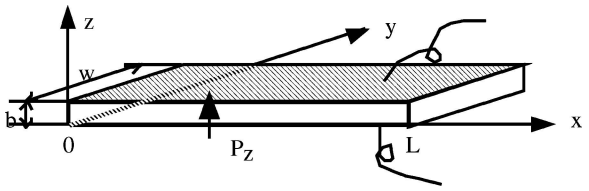

Figure 6 Longitudinal vibration through the transverse piezoelectric effect (d_{31}) in a rectangular plate.

characteristics through depoling of the piezoceramic. Therefore, the ultrasonic motor requires a very hard type piezoelectric with a high mechanical quality factor Q_m, leading to the suppression of heat generation. It is also notable that the actual mechanical vibration amplitude at the resonance frequency is directly proportional to this Q_m value.

3.1. Vibration at a piezoelectric resonance

Let us review the longitudinal mechanical vibration of a piezo-ceramic plate through the transverse piezoelectric effect (d_{31}) as shown in Fig. 6 [7]. Assuming that the polarization is in the z-direction and the x-y planes are the planes of the electrodes, the extensional vibration in the x direction is represented by the following dynamic equation:

$$(\partial^2 u/\partial t^2) = F = (\partial X_{11}/\partial x) + (\partial X_{12}/\partial y) + (\partial X_{13}/\partial z), \quad (32)$$

where u is the displacement of the small volume element in the ceramic plate in the x-direction. When the plate is very long and thin, X_2 and X_3 may be set equal to zero through the plate, and the following solutions can be obtained:

$$\text{(strain)} \quad \partial u/\partial x = x_1 = d_{31}E_Z[\sin\omega(L-x)/v + \sin(\omega x/v)]/\sin(\omega L/v), \quad (33)$$

$$\text{(total displacement)} \quad \Delta L = \int_0^L x_1 dx = d_{31}E_z L(2v/\omega L)\tan(\omega L/2v). \quad (34)$$

Here, v is the sound velocity in the piezoceramic which is given by

$$v = 1/\sqrt{\rho s_{11}^{\mathrm{E}}}. \quad (35)$$

The admittance for the mechanically free sample is calculated to be:

$$Y = (1/Z) = (i/V) = (i/E_z t) = (j\omega wL/t)\varepsilon_0\varepsilon_3^{\mathrm{LC}}[1 + (d_{31}^2/\varepsilon_0\varepsilon_3^{\mathrm{LC}}s_{11}^{\mathrm{E}}) \times (\tan(\omega L/2v)/(\omega L/2v)], \quad (36)$$

where w is the width, L the length, t the thickness of the sample, and V the applied voltage. $\varepsilon_3^{\mathrm{LC}}$ is the permittivity in a longitudinally clamped sample, which is given by

$$\varepsilon_0\varepsilon_3^{\mathrm{LC}} = \varepsilon_0\varepsilon_3^{\mathrm{X}} - \left(d_{31}^2/s_{11}^E\right) = \varepsilon_0\varepsilon_3^{\mathrm{X}}\left(1 - k_{31}^2\right). \quad (37)$$

Now, we will introduce the complex parameters into the admittance curve around the resonance frequency, in a similar way to the previous section: $\varepsilon_3^{\mathrm{X}*} = \varepsilon_3^{\mathrm{X}}(1 - j\tan\delta')$, $s_{11}^{\mathrm{E}^*} = s_{11}^{\mathrm{E}}(1 - j\tan\phi\prime)$, and $d_{31}^* = d(1 - j\tan\theta')$ into Equation 36:

$$Y = Y_{\mathrm{d}} + Y_{\mathrm{m}} = j\omega C_{\mathrm{d}}(1 - j\tan\delta) + j\omega C_{\mathrm{d}}K_{31}^2[(1 - j(2\tan\theta' - \tan\phi')] \times [(\tan(\omega L/2v^*)/(\omega L/2v^*)], \quad (38)$$

where

$$C_0 = (wL/t)\varepsilon_0\varepsilon_3^{\mathrm{X}}, \quad (39)$$

,

$$C_{\mathrm{d}} = \left(1 - k_{31}^2\right)C_0. \quad (40)$$

Note that the loss for the first term (damped conductance) is represented by the "extensive" dielectric loss $\tan\delta$, not by the intensive loss $\tan\delta'$. We further calculate $1/(\tan(\omega L/2v^*)$ with an expansion-series approximation around $(\omega L/2v)=\pi/2$, taking into account that the resonance state is defined in this case for the maximum admittance point.

Using new frequency parameters,

$$\Omega = \omega L/2v, \quad \Delta\Omega = \Omega - \pi/2(\ll 1), \quad (41)$$

and $K_{31}^2 = k_{31}^2/(1 - k_{31}^2)$, the motional admittance Y_{m} is approximated around the first resonance frequency by

$$Y_{\mathrm{m}} = j(8/\pi^2)\omega_0 C_{\mathrm{d}}K_{31}^2[(1 + j((3/2)\tan\phi' - 2\tan\theta')]/[(-(4/\pi)\Delta\Omega + j\tan\phi'). \quad (42)$$

The maximum Y_{m} is obtained at $\Delta\,\Omega = 0$:

$$Y_{\mathrm{m}}^{\max} = (8/\pi^2)\omega_0 C_{\mathrm{d}}K_{31}^2(\tan\phi')^{-1} = (8/\pi^2)\omega_0 C_{\mathrm{d}}K_{31}^2 Q_{\mathrm{m}}, \quad (43)$$

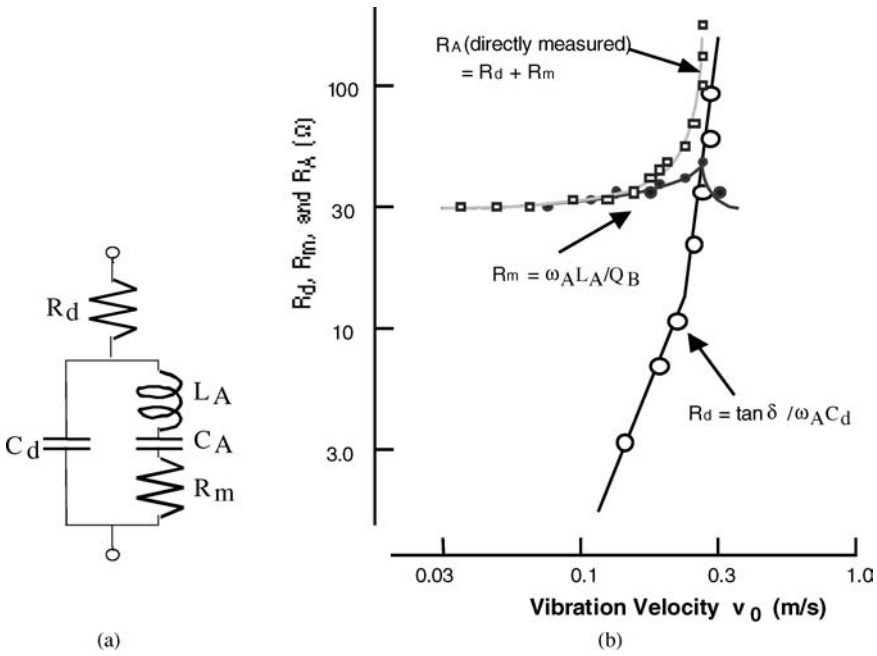

Figure 7 (a) Equivalent circuit of a piezoelectric device for the resonance under high power drive. (b) Vibration velocity dependence of the resistances R_d and R_m in the equivalent electric circuit for a longitudinally vibrating PZT ceramic transducer through the transverse piezoelectric effect d_{31}. Notice a dramatic change in R_d above a certain threshold vibration velocity.

where $Q_m = (\tan \phi')^{-1}$. Similarly, the maximum displacement u_{max} is obtained at $\Delta\Omega$=0:

$$u_{max} = (8/\pi^2) d_{31} E_Z L \, Q_m. \tag{44}$$

The maximum displacement at the resonance frequency is $(8/\pi^2)Q_m$ times larger than that at a non-resonance frequency, $d_{31}E_ZL$.

In a brief summary, when we observe the admittance or displacement spectrum as a function of drive frequency, and obtain the mechanical quality factor Q_m estimated from $Q_m = \omega_0/2\Delta\omega$, where $2\Delta\omega$ is a full width of the 3 dB down (i.e., $1/\sqrt{2}$) of the maximum value at $\omega = \omega_0$, we can obtain the intensive mechanical loss tan ϕ'.

3.2. Equivalent circuit under high power drive

The equivalent circuit for the piezoelectric actuator is represented by a combination of L, C and R. Fig.7a shows an equivalent circuit for the resonance state, which has very low impedance. Taking into account Equation 42, we can understand that C_d and R_d correspond to the electrostatic capacitance (for a longitudinally clamped sample in the previous case, not a free sample) and the clamped (or "extensive") dielectric loss tan δ, respectively, and the components L_A and C_A in a series resonance circuit are related to the piezoelectric motion. For example, in the case of the longitudinal vibration of the above rectangular plate through d_{31}, these components are represented approximately by

$$L_A = (\rho/8)(Lb/w)\left(s_{11}^{E2}/d_{31}^2\right), \tag{45}$$

$$C_A = (8/\pi^2)(Lw/b)\left(d_{31}^2/s_{11}^{E}\right). \tag{46}$$

The total resistance R_A (=$R_d + R_m$) should correspond to the loss tan ϕ', which is composed of the extensive mechanical loss tan ϕ and dielectric/piezoelectric coupled loss (tan $\delta - 2\tan\theta$) (see Equation 30). Thus, intuitively speaking, R_d and R_m correspond to the extensive dielectric and mechanical losses, respectively. Note that we introduced an additional resistance R_d to explain a large contribution of the dielectric loss when a vibration velocity is relatively large. There are, of course, different ways to introduce R_d in an equivalent circuit [8].

3.3. Losses as a function of vibration velocity

Let us consider here the degradation mechanism of the mechanical quality factor Q_m with increasing electric field and vibration velocity. Fig. 8 shows the change in mechanical Q_m with vibration velocity. Q_m is almost constant for a small electric field/vibration velocity, but above a certain vibration level Q_m degrades drastically, where temperature rise starts to be observed [9].

Fig. 7b depicts an important notion on heat generation from the piezoelectric material, where the damped and motional resistances, R_d and R_m, in the equivalent electrical circuit of a PZT sample (Fig. 7a are separately plotted

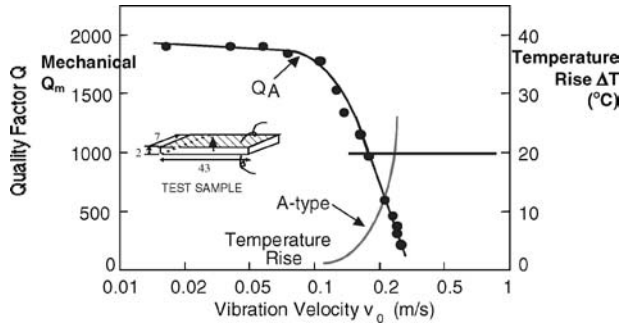

Figure 8 Vibration velocity dependence of the quality factor Q_A and temperature rise for A (resonance) type resonance of a longitudinally vibrating PZT ceramic transducer through the transverse piezoelectric effect d_{31}. The maximum vibration velocity is defined at the velocity where 20°C temperature rise from room temperature is exhibited.

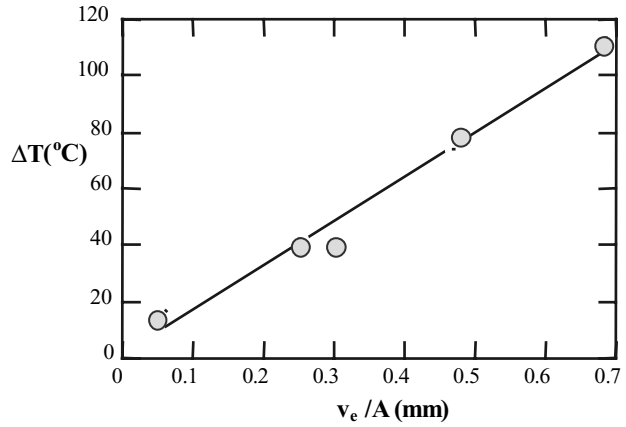

Figure 9 Temperature rise at off-resonance versus V_e/A (3 kV/mm, 300 Hz) in various size soft PZT multilayer actuators, where V_e is the effective volume generating the heat and A is the surface area dissipating the heat.

as a function of vibration velocity. Note that R_m, mainly related to the extensive mechanical loss (90° domain wall motion), is insensitive to the vibration velocity, while R_d, related to the extensive dielectric loss (180° domain wall motion), increases significantly around a certain critical vibration velocity. Thus, the resonance loss at a small vibration velocity is mainly determined by the extensive mechanical loss which provides a high mechanical quality factor Q_m, and with increasing vibration velocity, the extensive dielectric loss contribution significantly increases. This is consistent with the discussion made on Fig. 5. After R_d exceeds R_m, we started to observe heat generation.

4. Heat generation in piezoelectrics

Heat generation in various types of PZT-based actuators has been studied under a large electric field applied (1 kV/mm or more) at an off-resonance frequency and under a relatively small electric field applied (100 V/mm) at a resonance frequency.

Zheng *et al*. reported the heat generation at an off-resonance frequency from various sizes of multilayer type piezoelectric ceramic actuators [6]. The temperature change with time in the actuators was monitored when driven at 3 kV/mm and 300 Hz, and Fig. 9 plots the saturated temperature as a function of V_e/A, where V_e is the effective volume (electrode overlapped part) and A is the surface area. This linear relation is reasonable because the volume V_e generates the heat and this heat is dissipated through the area A. Thus, if we need to suppress the temperature rise, a small V_e/A design is preferred. From these experimental results, we calculated the total loss u of the piezoelectric, which is summarized in Table I. The experimental data of *P-E* hysteresis losses under a stress-free condition is also listed for comparison. It is very important that the *P-E* hysteresis intensive loss agrees well with the total loss contributing to the heat generation under an off-resonance drive.

Tashiro *et. al*. observed the heat generation in a rectangular piezoelectric plate during a resonating drive [10]. Even though the maximum electric filed is not very large, heat is generated due to the large induced strain/stress at the resonance. Fig. 10 depicted an infrared image taken for a resonating rectangular PZT plate in our laboratory. The maximum heat generation was observed at the nodal point of the resonance vibration, where the maximum strain/stress are generated. This observation supports that the heat generation in a resonating sample is attributed to the intensive elastic loss tan ϕ'. This is not contradictory to the result in the previous paragraph, where a high-voltage was applied at an off-resonance frequency. We concluded there that the heat is originated from the intensive dielectric loss tan δ'. In consideration that both the "intensive" dielectric and mechanical losses are composed of the "extensive" dielectric and mechanical losses, and that the extensive dielectric loss tan δ changes significantly with the external electric field and stress, the major contribution to the heat generation seems to come from the "extensive" dielectric loss (i.e., 180° domain wall motion). Since this is just our model, there can be different domain reorienta-

TABLE I Loss and overall heat transfer coefficient for PZT multilayer samples ($E = 3$ kV/mm, $f = 300$ Hz). The effective heat transfer coefficient here is the sum of the rates of heat flow by radiation and by convection, neglecting the conduction effect

Actuator	4.5×3.5×2 mm	7×7×2 mm	17×3.5×1 mm
Total loss ($\times 10^3$ J/m^3) $u = \frac{\rho cv}{f v_e}\left(\frac{dT}{dt}\right)_{t-} > 0$	19.2	19.9	19.7
P-E hysteresis loss ($\times 10^3$ J/m^3)	18.5	17.8	17.4
$k(T)$ (W/m^{2}K)	38.4	39.2	34.1

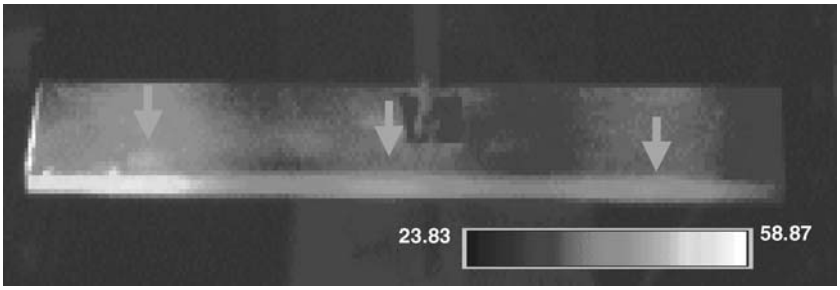

Figure 10 An infrared image of a "hard" PZT rectangular plate driven at the second resonance mode. Note three hot points, which correspond to the nodal points for this vibration mode.

tion models, and further investigations are waited for the microscopic observation of this phenomenon.

5. High power piezoelectrics

5.1. Practical PZT based ceramics

"High Power" in this paper stands for high power density in mechanical output energy converted from the maximum input electrical energy under the drive condition with 20°C temperature rise. The mechanical power density can be evaluated by the square of the maximum vibration velocity (v_0^2), which is a sort of material's constant (Remember that there exists the maximum mechanical energy density, above which level, the piezoelectric material becomes a ceramic heater.). Fig. 11 shows the mechanical Q_m versus basic composition x at two effective vibration velocities $v_0 = 0.05$ m/s and 0.5 m/s for $Pb(Zr_xTi_{1-x})O_3$ doped with 2.1 at % of Fe [11]. The decrease in mechanical Q_m with an increase of vibration level is minimum around the rhombohedral-tetragonal morphotropic phase boundary (52/48). In other words, the smallest Q_m material under a small vibration level becomes the highest Q_m material under a large vibration level, and the data obtained by a conventional impedance analyzer with a small voltage/power does not provide data relevant to high power characteristics. Thus, we developed various measuring techniques of high power piezoelectricity, including "Constant Current" and "pulse drive" methods [12].

The conventional piezo-ceramics have the limitation in the maximum vibration velocity (v_{max}), since the additional input electrical energy is converted into heat, rather than into mechanical energy. The typical rms value of v_{max} for commercially available materials, defined by the temperature rise of 20°C from room temperature, is around 0.3 m/sec for rectangular samples operating in the k_{31} mode (like a Rosen-type transformer) [9]. $Pb(Mn,Sb)O_3$ (PMS) – lead zirconate tatanate (PZT) ceramics with the v_{max} of 0.62 m/sec are currently used for NEC transformers [11]. By doping the PMS-PZT or $Pb(Mn,Nb)O_3$-PZT with rare-earth ions such as Yb, Eu and Ce, we recently developed the high power piezoelectrics, which can operate with v_{max} up to 1.0 m/sec [13, 14]. Compared with commercially available piezoelectrics, 10 times higher input electrical energy and output mechanical energy can be expected from these new materials without generating significant temperature rise, which corresponds to 100 W/cm^2. Fig. 12 shows the dependence of the maximum vibration velocity v_0 (20°C temperature rise) on the atomic % of rare-earth ion, Yb, Eu or Ce in the $Pb(Mn,Sb)O_3$ (PMS) – PZT based ceramics. Enhancement in the v_0 value is significant by adding a small amount of the rare-earth ion [14].

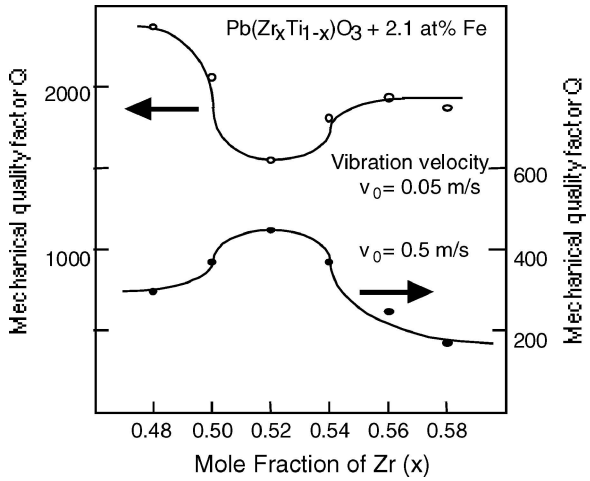

Figure 11 Mechanical Q_m versus basic composition x at two effective vibration velocities $v_0 = 0.05$ m/s and 0.5 m/s for $Pb(Zr_xTi_{1-x})O_3$ doped with 2.1 at % of Fe.

5.2. Origin of the high power piezoelectrics

"Hard" PZT is usually used for high power piezoelectric applications, because of its high coercive field; in other words, the stability of the domain walls. Acceptor ions, such as Fe^{3+}, introduce oxygen deficiencies in the PZT crystal (In the case of donor ions, such as Nb^{5+}, Pb deficiency is introduced). Thus, in the conventional model, the acceptor doping causes domain pinning through the easy reorientation of deficiency-related dipoles, leading to "hard" characteristics (Domain Wall Pinning Model

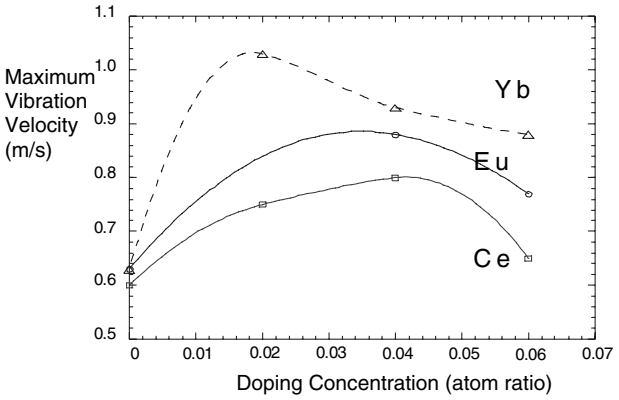

Figure 12 Dependence of the maximum vibration velocity v_0 (20°C temperature rise) on the atomic % of rare-earth ion, Yb, Eu or Ce in the $Pb(Mn,Sb)O_3$ (PMS) – PZT based ceramics.

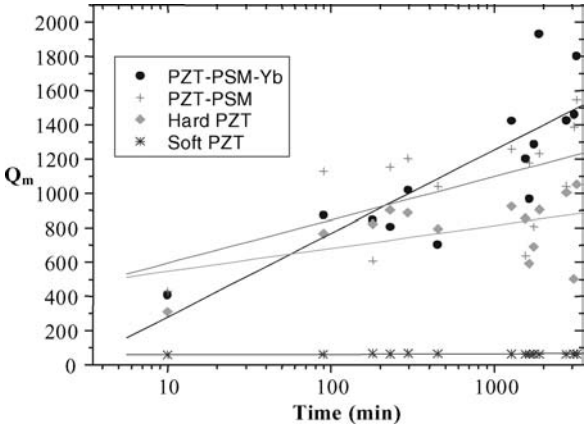

Figure 13 Change in the mechanical Q_m with time lapse (minute) just after the electric poling measured for various commercial soft and hard PZTs, PSM-PZT, and PSM-PZT doped with Yb.

[15]). In this section, we explore the origin of our high power piezoelectric ceramics.

High mechanical Q_m is essential in order to obtain a high power material with a large maximum vibration velocity. Fig. 13 exhibits suggestive results in the mechanical Q_m increase with time lapse (minute) after the electric poling measured for various commercial soft and hard PZTs, PSM-PZT, and PSM-PZT doped with Yb. It is notable that the Q_m values for commercial hard PZT and our high power piezoelectrics were almost the same, slightly higher than soft PZTs, and around 200–300 immediately after the poling. After a couple of hours passed, the Q_m values increased more than 1000 for the "hard" materials, while no change was observed in the "soft" material. The increasing slope is the maximum for the Yb-doped PSM-PZT. We also found a contradiction that this gradual increase (in a couple of hours) in the Q_m cannot be explained by the above-mentioned "domain wall pinning" model, but more likely by some ionic diffusion model.

Fig. 14 shows the polarization vs. electric field hysteresis curves measured for the Yb-doped $Pb(Mn,Sb)O_3$- PZT sample immediately after poling (fresh), 48 hr after, and a week after (aged). Remarkable aging effects could be observed; (a) in the decrease in the magnitude of the remnant polarization, and (b) in the positive internal bias electric field growth (i.e., the hysteresis curve shift leftwards in terms of the external electric field axis). The phenomenon (a) can be explained by the local domain wall pinning effect, but the large internal bias (more than 1 kV/mm) growth (b) seems to be the origin of the high power characteristics. Suppose that the vertical axis in Fig. 5 shifts rightwards, the inverse electric field required for realizing the 180° polarization reversal is increased, leading to the resistance enhancement against generating the hysteresis or heat.

Finally, let us propose the origin of this internal bias field growth. Based on the necessity of the oxygen deficiencies and the relatively slow (a couple of hours) growth rate, we assume here the oxygen deficiency diffusion model, which is illustrated in Fig.15. Under the electric poling process, the defect dipole P_{defect} (a pair of acceptor ion and oxygen deficiency) will be arranged parallel to the external electric field. After removing the field, the oxygen diffusion occurs, which can be estimated in a scale of hour at room temperature. Taking into account slightly different atomic distances between the A and B ions in the perovskite crystal in a ferroelectric (asymmetric) phase, the oxygen diffusion probability will be slightly higher for the downward, as shown in the figure, leading to the increase in the defect dipole with time. This may be the origin of the internal bias electric field.

6. High power piezoelectric components

Though we have developed "high power density" piezoelectric ceramics, the multilayer structure is a key to develop actual "high power" components from the device designing viewpoint. However, the present Ag-Pd electrode structure includes two-fold problems; (1) expensive Pd, and (2) Ag migration under a high field. In order to solve the problems, pure Cu electrode will be a key. But, the multilayer samples need to be sintered at a relatively low temperature (900°C or lower), when utilizing Cu embedded electrodes. Thus, low temperature sintering of "hard" type PZTs is a necessary technology to be developed. Different from soft PZTs, most of the conventional dopants to decrease the sintering temperature failed to be used, because these dopants also degrade the Q_m value significantly.

Our recent development of multilayered piezoelectric transformers with a hard piezoelectric ceramic is introduced here. In this sort of electric-mechanical-electric conversion application (combination of the converse and direct piezoelectric effects), since the fig. of merit is v_0k, the composition needs to sustain high d

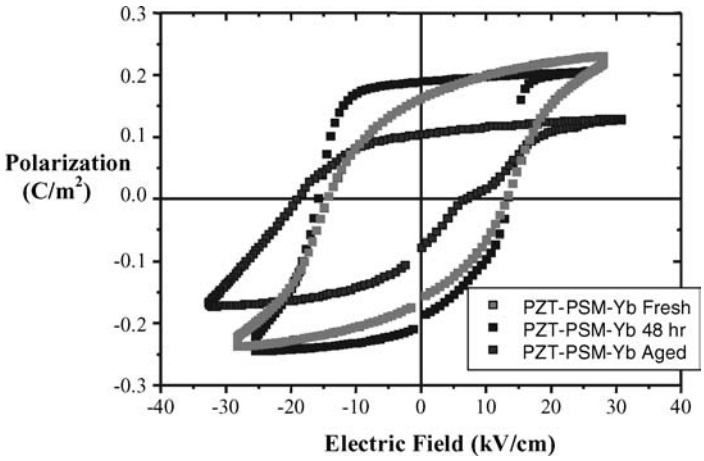

Figure 14 Polarization vs. electric field hysteresis curves measured for the Yb-doped $Pb(Mn,Sb)O_3$- PZT sample just after poling (fresh), 48 hours after, and a week after (aged).

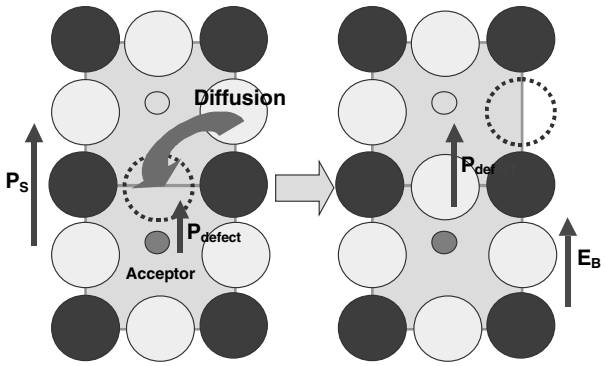

Figure 15 Oxygen deficiency diffusion model for explaining the internal bias electric field growth.

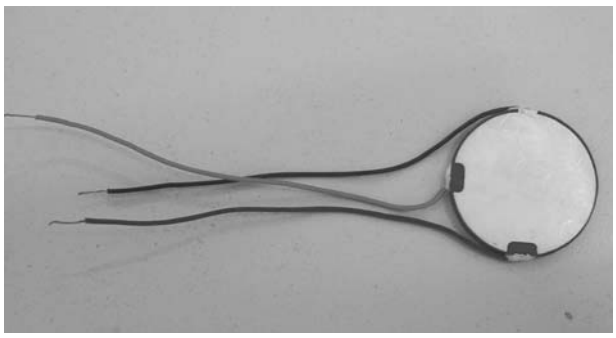

Figure 16 Multilayer co-fired transformer (35 W) with "hard" PZT and pure Ag electrodes, sintered at 880°C [Penn State trial product].

and k by keeping reasonable maximum vibration velocity. From the above reason, a new hard PZT composition system has been tried, starting from the originally soft $Pb(Zn_{1/3}Nb_{2/3})_x(Zr_{0.5}Ti_{0.5})_{1-x}O_3$. The composition corresponding to 0.2 PZN−0.8 PZT+0.5 wt% MnO_2 was found to have high piezoelectric properties along with a reasonable mechanical quality factor (d_{33}=277 pC/N, $\varepsilon_{33}/\varepsilon_o$=946, tan δ'=0.35%, k_p=0.58, Q_m=1402, $v_{0,rms}$=0.55 m/s). Furthermore, we found that modification of 0.2 PZN−0.8 PZT+0.5 wt% MnO_3 with $PbTiO_3$ and CuO lowered the sintering temperature to 880°C [See Table II]. The low field piezoelectric properties of the sample sintered at 880°C for 2 hr were found to be as: d_{33}=300 pC/N, $\varepsilon_{33}/\varepsilon_o$=1100, tan δ'=1.2%, k_p=0.52 and Q_m=900. Cu-embedded multilayer transformers are now being developed in trial as depicted in Fig. 16.

7. Conclusions

(1) There are three loss origins in piezoelectrics: dielectric, elastic and piezoelectric losses. 180° and non-180° domain wall motions contribute primarily to the extensive dielectric and elastic losses, respectively.

(2) Heat generation occurs in the sample uniformly under an off-resonance mainly due to the intensive dielectric loss, while heat is generated primarily at the vibration nodal points via the intensive elastic loss under a resonance. In both cases, the loss increase is originated from the extensive dielectric loss change with electric field and/or stress.

(3) Doping rare-earth ions into PZT-$Pb(Mn,X)O_3$ (X = Sb, Nb) ceramics increases the maximum vibration velocity up to 1 m/s, which corresponds to one order of magni-

TABLE II Electromechanical coupling parameters for low temperature sintering "hard" PZT based ceramics: 0.2 PZN−0.8 PZT + 0.5 wt% MnO_2 with $PbTiO_3$ and CuO

wt% PT extra	Sintering Temp.(°C)	k_p	Q_m	d_{33} (pC/N)	$\varepsilon_{33}/\varepsilon_0$	tan δ (%)
0	1200	0.55	1502	265	1011	0.56
6.5	1000	0.47	1308	260	1300	1
6.3 + 0.3 wt% CuO	880	0.52	900	300	1100	1.2

tude higher energy density than conventionally commercialized piezo-ceramics.

(4) To obtain high power density/high vibration velocity materials, domain wall immobility/stabilization via the positive internal bias field seems to be essential, rather than the local domain wall pinning effect.

Since the above conclusions were derived only from a limited number of PZT-based soft and hard piezoelectrics, it is too early to generalize these conclusions. Further investigations are highly required.

Acknowledgments

Part of this research was supported by the Office of Naval Research through the grant no. N00014-96-1-1173 and N00014-99-1-0754.

References

1. K. H. HAERDTL, *Ceram. Int'l.* **8** (1982) 121.
2. T. IKEDA, "Fundamentals of Piezoelectric Materials Science", (Ohm Publication Co., Tokyo, 1984) 83.
3. N. SETTER, (ed.) *Piezoelectric Materails in Devices*, (2002).
4. K. UCHINO and S. HIROSE, *IEEE-UFFC Trans.* **48** (2001) 307.
5. J. ZHENG, S. TAKAHASHI, S. YOSHIKAWA, K. UCHINO and J. W. C. DE VRIES, *J. Amer. Ceram. Soc.* **79** (1996) 3193.
6. N. UCHIDA and T. IKEDA, *Jpn. J. Appl. Phys.* **6** (1967) 1079.
7. K. UCHINO, "Piezoelectric Actuators and Ultrasonic Motors", (Kluwer Academic Publ., Boston, 1997) p. 197.
8. M. UMEDA, K. NAKAMURA and S. UEHA, *Jpn. J. Appl. Phys.* **38** (1999) 3327.
9. S. HIROSE, M. AOYAGI, Y. TOMIKAWA, S. TAKAHASHI and K. UCHINO, *Proc. Ultrasonics Int'l '95*, Edinburgh, (1995) 184.
10. S. TASHIRO, M. IKEHIRO and H. IGARASHI, *Jpn. J. Appl. Phys.* **36** (1997) 3004.
11. S. TAKAHASHI and S. HIROSE, *ibid.* **32** (1993) 2422.
12. K. UCHINO, J. ZHENG, A. JOSHI, Y. H. CHEN, S. YOSHIKAWA, S. HIROSE, S. TAKAHASHI and J. W. C. DE VRIES, *J. Electroceramics* **2** (1998) 33.
13. J. RYU, H. W. KIM, K. UCHINO and J. LEE, *Jpn. J. Appl. Phys.* **42**(3) (2003) 1.
14. Y. GAO, K. UCHINO and D. VIEHLAND, *J. Appl. Phys.* **92** (2002) 2094.
15. K. UCHINO, "Ferroelectric Devices" (Marcel Dekker, Inc., New York, 2000), p. 63.